

## IMPROVING CITY MODEL DETERMINATION BY USING ROAD DETECTION FROM LIDAR DATA

S. P. Clode<sup>a,\*</sup>, F. Rottensteiner<sup>b</sup>, P. Kootsookos<sup>c</sup>

<sup>a</sup> IRIS Group, EMI, University of Queensland, Brisbane, QLD 4072, AUSTRALIA - sclode@itee.uq.edu.au

<sup>b</sup> School of Surveying and SIS, UNSW, Sydney, NSW 2052, AUSTRALIA - f.rottensteiner@unsw.edu.au

<sup>c</sup> United Technologies Research Center, Silver Lane, USA US - KootsoPJ@UTRCCT.res.utc.com

### Commission III, WG III/4

**KEY WORDS:** ALS, Bridges, Buildings, City Models, Roads, LIDAR

#### ABSTRACT:

A new road classification technique from Light Detection And Ranging (LIDAR) data is presented that relies on region growing in order to classify areas as road. The new method corrects some of the problems encountered with previously documented LIDAR road detectors. A major benefit of the new road detection method is that it can be combined with standard building detection techniques to detect bridges within the road network. As a consequence bridges are identified as false positive detections in the candidate building regions and can be removed, thus improving the obtained building mask whilst more detail is added to the final classification scheme seen in the road network. Vectorisation of the detected road network is performed using a Phase Coded Disk (PCD) thus completing the detection and vectorisation processes. The benefits of using LIDAR data in road extraction is emphasised by the simple but automated creation of longitudinal profiles and cross sections from the vectorised road network.

### 1. INTRODUCTION

#### 1.1 Motivation and Aims

In contrast to the well studied problem of building detection and reconstruction from Light Detection And Ranging (LIDAR) data (Brunn and Weidner, 1997; Haala and Brenner, 1999; Rottensteiner and Briese, 2002; Rottensteiner, et al., 2003), the detection of roads from LIDAR is in its infancy (Clode et al., 2004b). The demand for automatic road extraction is driven by the importance of maintaining Geographic Information Systems (GIS) (Fuchs et al., 1998). Road detection from remotely sensed data is a difficult problem that requires more research due to the many unsolved questions related to scene interpretation (Hinz and Baumgartner, 2003). Existing road extraction techniques are characterised by poor detection rates and the need for existing data and / or user interaction (Zhang, 2003; Hatger and Brenner, 2003). The aims of this paper are to improve current road detection techniques from a single data source, namely LIDAR data, combine building and road detection techniques to help identify bridges within the road network and to vectorise the detected road network. Additionally, the paper aims to highlight the need for the development of the ontology between spatial classes within an urban scene by introducing building and vegetation detection into the road detection algorithm. In this context, ontology is a description of the concepts and relationships that exist for a spatial class or a set of spatial classes.

This section will continue with a review of related work. Existing road model assumptions are discussed and put in perspective. Section 2 describes the new approach and discusses differences in road model assumptions. Section 3 discusses the vectorisation method used, namely the Phase Coded Disk

(PCD) and describes some benefits of using LIDAR to detect roads as compared with other remotely sensed data sources. Results from the two sample data sets are discussed in section 4 whilst conclusions and future work are examined in section 5.

#### 1.2 Related Work

The increased use and reliance on GIS within the spatial information community has stimulated research on automated road extraction (Hinz and Baumgartner, 2003). The extraction of roads from optical or RADAR imagery is a well studied problem summarized well by Auclair-Fortier et al. (2000) and by Zhang (2003). The task of road extraction from remotely sensed data involves two distinct steps, classification and vectorisation or road parameter determination. There are many difficulties associated with extracting roads from aerial images; the basic task of road extraction from LIDAR is similar to methods used to extract roads from other remotely sensed data.

LIDAR is a relatively new technology that has the ability to acquire very dense point clouds in a short period of time (Kraus, 2002). A consequence of this infancy combined with the difficulty of road extraction in general, is that there have been relatively few attempts to extract roads from LIDAR data. Most attempts have required a form of data fusion to complete the task such as in (Hatger and Brenner, 2003). Road geometry parameters were estimated by combining high resolution LIDAR data (4 points per m<sup>2</sup>) and an existing database to derive the height, slope, curvature and width of the road. The road centreline was provided by the existing database. The centreline is essential to the definition of a road and was used to extract the other road parameters but ultimately the primary road definition was not provided by the LIDAR data.

\* Corresponding author.

High resolution LIDAR data was used by Rieger et al. (1999) in forested areas to extract road information. The roads were initially detected in order to generate breaklines to enhance the quality of the previously determined Digital Terrain Model (*DTM*). The road network was modelled by pairs of parallel edges that were identified using “twin snakes” and line and point feature extraction. The connection between road network models and *DTM*'s is highlighted by Akel et al. (2003) where *DTM*s in urban areas are extracted by initially estimating the *DTM* from the road network present. The interesting model assumption is made that roads lie on the *DTM*.

The success of a road extraction technique is largely dependant on the suitability or degree of approximation of the road model to adequately represent the road network being detected. As described by Zhang (2003) the selection of a road model is dependant of the appearance of a road in the sensor data. Auclair-Fortier et al. (2000) identified four different categories by which road characteristics could be classified, namely, spectral, geometric, topologic and contextual. It seems natural that a successful road detection model would address each of the different categories.

The fact that LIDAR data is an explicit 3D data source means that model assumptions pertaining to each dimension are quite feasible. For instance, the assumption that a road network lies on the *DTM* is valid and to some extent addresses the geometric properties of a road. In our previous work, this geometric assumption was used to first filter out last-pulse LIDAR positions that coincided or almost coincided with the *DTM* (Clode et al., 2004b). Model assumptions relating to both spectral and contextual characteristics are then applied to only this subset of data. By means of prior knowledge, a valid range of acceptable laser intensity values that adequately represent the reflectivity of the road surface is initially determined. The subset is then further thinned based on this spectral criterion. A local point density is then calculated, whereby the number of points in the local neighbourhood is compared to a simple threshold value to find all the LIDAR strikes that fit the road model assumptions. Thus the contextual characteristics have been fulfilled. As (Clode et al., 2004b) only deals with the classification of roads on a pixel by pixel basis, the topologic characteristics have been ignored in the model assumptions. The results presented were very promising but the authors highlighted some deficiencies in their model assumptions, especially with bridges, where the definition of the “terrain” is ambiguous. Interestingly, bridges were also noticed to be an error source in building detection, because they are higher than the *DTM* (if the *DTM* is defined to represent the lowest terrain surface) and have a smooth surface (Rottensteiner et al., 2003). This ambiguity is inherent in the definition of a bridge: on the one hand, bridges are man-made objects similar to buildings, and on the other hand, they are part of the road network. The paper presented here highlights this relationship between road and building detection and questions whether one can be performed successfully without the other.

The second problem in road extraction is vectorisation. One of the most common techniques used in vectorisation is the Hough or Radon Transform (Duda and Hart, 1972). Roads appear as either relatively thin lines in low resolution data or as two-dimensional areas with both width and length, in high resolution data. As LIDAR data is classified as high resolution in this context, the centre line of the road can not be extracted directly as the centreline is not the longest line in the image (Clode et al., 2004a). Scale space methods have been used to reduce this effect. The Phase-Coded-Disk (PCD) overcomes these problems as discussed in (Clode et al., 2004a) and will be used in this paper to vectorise the final road network.

## 2. CLASSIFICATION OF ROADS IN CITY SCENES

### 2.1 Pre-processing

A last pulse Digital Surface Model (*DSM*) is created from the original LIDAR points using inverse distance weighting. A gradient image is then created by differentiating the *DSM*. A *DTM* is created using morphologic filtering in a hierarchical framework that commences by creating an initial coarse *DTM* from the one large structural element. A rule-based algorithm is then applied to detect large buildings in the data (Rottensteiner et al. 2003). A smaller structural element is used to create a finer *DTM*, but buildings detected in the previous iteration have there corresponding heights substituted from *DTM* of the previous iteration. The process is continued until a minimum size for the structural element is reached. In order to remove any of the residual artefacts caused by the smallest structural element size, the final *DTM* is created by re-interpolating the surface but excluding LIDAR points classified as “off-terrain”. A normalised *DSM* (*nDSM*) identifying areas that lie above the terrain is created:

$$nDSM = DSM - DTM \quad (1)$$

We also compute an intensity density image  $I_\rho$  according to

$$I_\rho = \frac{|\{p_j \in S_1 : \|p_k - p_j\|_2 < d\}|}{|\{p_j \in S : \|p_k - p_j\|_2 < d\}|} \quad (2)$$

where  $p_k$  is the spatial location of the grid point being interpolated,  $p_j$  is the spatial location of the last-pulse LIDAR data point,  $d$  is the size of the local neighbourhood and  $S$  and  $S_1$  are the set of all LIDAR points and all LIDAR points with the intensity matching the spectral properties of the road surface to be detected. By using the density function some of problems caused by noise within the intensity image as described in (Vosselman, 2002) can be overcome.

Using the *nDSM* and surface roughness parameters, buildings are detected by a rule-based algorithm similar to (Rottensteiner, 2003). As we shall see in section 2.2, the results of building detection will help to detect bridges. Vegetation is also detected using the algorithm described in (Clode et al., 2005). The tree outlines are generated from the local point density of points within the local neighbourhood that have registered a difference between the first- and last- pulse laser strikes. A more stringent density is required in order to classify a tree so that the overhanging areas over a road can still be classified as road but not have the road pass through the centre of the treed area. The detected trees will be used to determine a stopping criterion for region growing in the road detection algorithm.

### 2.2 The Road Detection Algorithm

We propose a region growing algorithm for the detection of the road network that assumes a similar road model to the one described in (Clode et al., 2004b). As pointed out in section 1.2, that model exploits the continuous homogeneous nature of a road by using the normalised local point density of LIDAR points that lie on or near the *DTM* and meet certain reflectance requirements in the wavelength of the ALS system. We have improved the original algorithm by considering the results of building and vegetation extraction, thus overcoming problems caused by bridges and by vegetation overhanging roads.

The region growing algorithm scans the image for a seed point that meets the criteria set out in Clode et al. (2004b). The requirements are that the seed point must lie on or near the *DTM* and the spectral density requirements meet the required

percentage of the local neighbourhood. Once a valid seed point is identified, the region attempts to grow by testing the neighbouring pixels based on three criteria: (1) The percentage of LIDAR points in the local neighbourhood that have similar spectral properties must be above a certain threshold. (2) The pixel must not be classified as a tree and (3) the change in height between the current pixel and the pixel to be added to the region must not exceed a predefined threshold. A region will grow until no further pixel can be added to it. Once the region is complete, another seed point is sought until the image has been completely interrogated.

On completion of a region growing, the percentage of the region that lies on or near the *DTM* compared to the overall region size is calculated and is accepted if it is less than as predefined threshold. This threshold is data dependant as the size and number of bridges within a road network will affect this value. In areas where elevated roads exist, the threshold will need to be set much lower to allow the region to be accepted. At this time the size of the grown region is also checked to ensure that the region is not just noise. Small regions are removed. Finally the size of each region is compared to its bounding rectangle and regions with a low area ratio are removed. In the final road segments, small gaps are removed by labelling the inverse of the road image and removing small components. By combining the detected road segments and the candidate building regions, bridge pixels are detected where a road segment and a building region overlap. Groups of pixels are labelled using connected component analysis to ultimately identify potential bridges. Areas classified as bridges provide extra information about the detected roads, in particular in areas where a road passes over another road. The presence of bridges in this scenario will determine whether a junction is formed. Detected bridges are also removed from the building image.

### 3. VECTORISATION

#### 3.1 The PCD

In order to satisfy the final road characteristic set out in (Auclair-Fortier et al., 2000) vectorisation of the road must be performed. Vectorisation of the classified image can be achieved by using the methods described in (Clode et al., 2004a) where a PCD (figure 1a) is convolved with the binary classified road image. The result of this convolution is a phase and magnitude image allowing the centreline, direction and width of the road all to be calculated. The benefit of the PCD over other line detection methods is that it will detect the centreline of a thick line (road) rather than the longest line in the image as in the case of the Hough or Radon Transform (Clode et al., 2004a).

The PCD used is defined by  $O_{PCD} = e^{j2 \cdot \tan^{-1}(y/x)} = e^{j2\vartheta}$  where  $x^2 + y^2 \leq r^2$ ,  $\vartheta = \tan^{-1}(y/x)$  and  $r$  is the radius of the disk. The PCD takes a convolution approach to centreline detection by convolving  $O_{PCD}$  with the binary image  $F(x,y)$  of road pixels. Figure 1 shows a constructed PCD and how the disk will be overlaid on a binary road image during the convolution process. The result of the convolution yields a magnitude ( $M$ ) and a phase image ( $P$ ) which are defined by equation 3:

$$\begin{aligned} M &= |F(x,y) \otimes O_{PCD}| \\ P &= \arg(F(x,y) \otimes O_{PCD}) \end{aligned} \quad (3)$$

Clode et al. (2004a) describe three important relationships that relate the road parameters to the convolution results: (1) the relationship between the centreline of the road and the peak of the magnitude image, (2) the width of the road and the magnitude image and (3) the direction of the line and the phase image. The magnitude can be shown to be a function of the

width of the road as described in equation 4 at any point that corresponds to the centreline of the road (which is represented by a peak in the magnitude image). The phase at any position represents twice the directional angle  $\phi$  of the underlying road. The relationships are described by Figure 1b where  $w$  is the width of the road,  $r$  is the radius of the PCD and  $\phi$  is the direction of the road.

$$\begin{aligned} M &= \left| w^2 \cos^{-1}\left(\frac{w}{2r}\right) - 2w \sqrt{r^2 - \frac{w^2}{4}} \right| \\ \phi &= \frac{1}{2} \arg(F(x,y) \otimes O_{PCD}) \end{aligned} \quad (4)$$

To extract the road centrelines the magnitude image is masked with the binary road mask to remove noise. A seed point is created for the tracing algorithm at the maximum value in the image and the corresponding line direction is read from the phase image. Tracing occurs by moving through the image pixel by pixel ensuring that the point is still a maximum against its neighbours until the line ends at a pixel of zero magnitude. Points either side of the traced line within the calculated road width are zeroed as the centreline is traced to ensure that a similar path is not retraced. The process is completed in the diametrically opposed line direction to complete the line tracing. This process is continued until all lines have been traced. Neighbouring centreline segments are then joined according to their direction and intersection locations to ensure that road centrelines that were traced with more than one seed are represented as a single continuous road. Intersections are created in areas where a road join passes over another centreline in areas where a bridge is not present. Road edge positions are calculated for all points along each centreline as determined by the road width and direction and is described in section 3.2 in more detail.

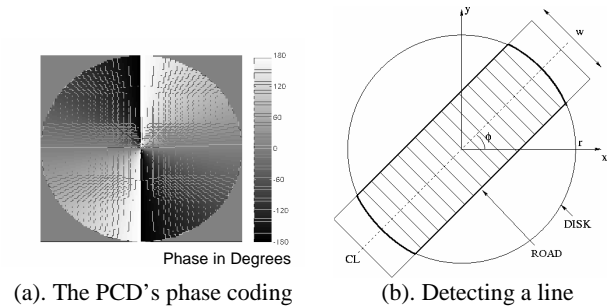


Figure 1. The Phase Coded Disk

#### 3.2 Generation of longitudinal sections and Cross sections.

Longitudinal profiles are obtained by sampling the *DSM* heights along the centreline at the predetermined interval. Cross-sections are generated at every longitudinal point by obtaining the *DSM* height values along the cross section at the point. The cross section is calculated by first obtaining the width of the road and the direction of the road  $\phi$  (equation 4). The road width is then smoothed by applying a low pass filter to the widths of each position on the road centreline. Cross section points are generated by calculating the offsets spacing at a direction based on the road direction plus or minus  $90^\circ$ . All offset values can then be plotted in a single cross section.

## 4. RESULTS

#### 4.1 The Test Data Sets

Two data sets are used in this paper to demonstrate the proposed algorithm. Both data sets are from Australia, namely Fairfield (NSW), and Yeronga (QLD). The average point density of the data sets is one point per 1.3 and 0.5  $m^2$ ,

respectively. In order to evaluate the road classification, ground truth data for the road networks were obtained by manually digitising the roads in an orthophoto of the area. The resultant ground truth images are displayed in Figures 2(a) and 2(c).

## 4.2 The Detected Road Network

**4.2.1 Classification Results:** The results of the classification can be visually inspected in Figures 2(b) and 2(d). The classification results were then compared directly to the digitised ground truth in order to measure the success of the classification method. Each pixel was classified in terms of being true positive (TP), false negative (FN) or false positive (FP), and the completeness, the correctness and the quality of the results were determined, based on Heipke (1997), according to Equation 5:

$$\begin{aligned} \text{Completeness} &= \frac{TP}{TP + FN} \\ \text{Correctness} &= \frac{TP}{TP + FP} \\ \text{Quality} &= \frac{TP}{TP + FP + FN} \end{aligned} \quad (5)$$

The results of the algorithm presented in this paper are presented in Table 1. These results can be directly compared to the results of the algorithm presented in (Clode et al., 2004b) as both the same data and ground truth were used. The results from this algorithm are presented in Table 2. The results of the new region growing algorithm appear to yield similar results than the algorithm described in (Clode et al., 2004b) with the additional benefit of not requiring a hard threshold with respect to the *DTM*. This improvement has allowed potential bridges to be identified in the data sets. The similarity of results was expected as the model assumptions were similar in both methods.

	Completeness	Correctness	Quality
Fairfield	0.87	0.70	0.63
Yeronga	0.73	0.85	0.65

Table 1. Quality Results from the region growing algorithm

	Completeness	Correctness	Quality
Fairfield	0.86	0.69	0.62
Yeronga	0.79	0.80	0.66

Table 2. Quality Results from the workflow in Clode (2004b)

## 4.3 Bridges

From the method detailed in Section 2.2 there were 5 potential bridges detected in the Fairfield data set and 6 potential bridges detected from the Yeronga data set. The spatial location of each detected bridge is shown in Figure 3. Each bridge has been labelled and identified with a blue arrow to assist the reader.

A visual inspection of the Fairfield data set yielded four (4) bridges within the area. These bridges are labelled 1, 2, 3 and 4 in Figure 3a and are displayed in Figure 4 to provide the reader with an understanding of the types and nature of bridges being detected. The bridge labelled 5 in the Figure 3a appears to be a false positive detection. From the orthophoto the area appears to be an elevated car park that was classified as road.

After a visual inspection of the Yeronga orthophoto it was concluded that there were five (5) bridges in the area which consisted of four bridges in the road network and 1 in the railroad network. These bridges are labelled 6, 7, 8 and 11 in Figure 3b and are displayed in Figure 4. There were 2 false positive bridge detections. The two false positives coincide with detected bridges 9 and 10 and appear on either side of bridge 6. Differences between the *DSM* and *DTM* have caused the

problem in these areas of sharp rises in terrain. It is anticipated that a more accurate *DTM* would fix these two false positive detections. In Figure 4(g) bridge 8 is the bridge in the left hand side of the image. On the right hand side the fourth of the road network bridges is found. This bridge was not detected by the algorithm probably because the height was too low to be registered as a building. Bridge 11 is a railroad bridge and this was not contained in the ground truth data as only roads were digitised.

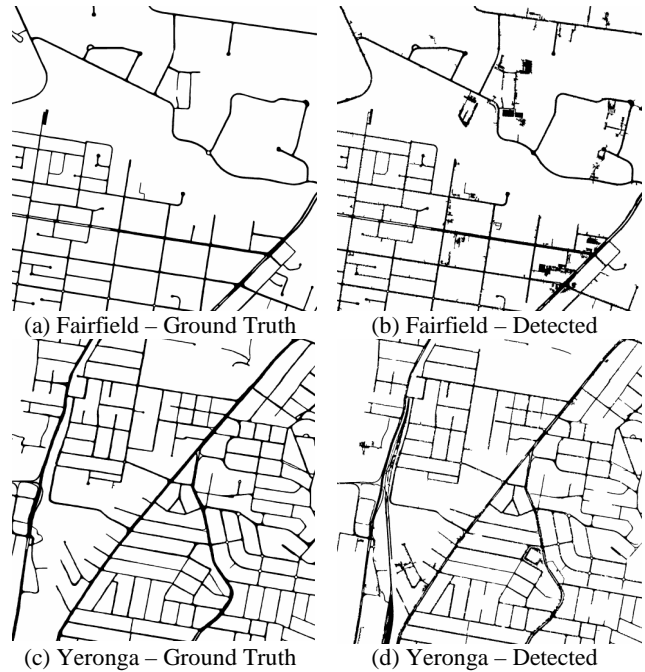


Figure 2. Ground truth and results for both the data sets

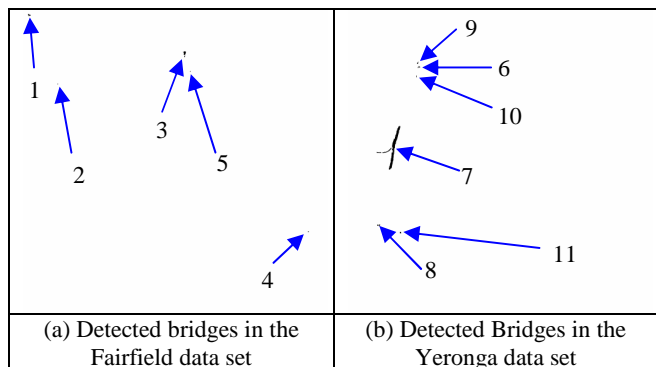


Figure 3. Detected Bridges

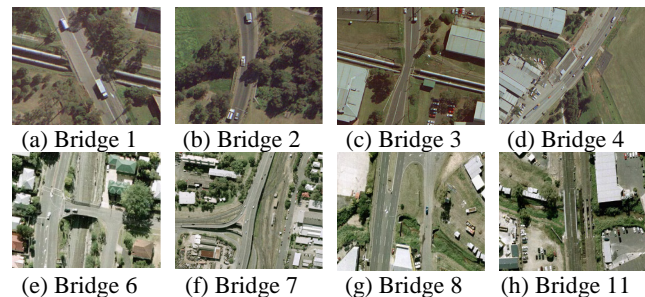


Figure 4. Manually identified bridges within the Fairfield (above) and Yeronga (below) data sets

## 4.4 Building Detection

One of the additional benefits to this method is the reduction in the number of false positive detections caused by bridges in the building image. A candidate building image is generated by the methods detailed in (Rottensteiner et al., 2003) (cf. Figure 5a

for the Yeronga data set). Figure 5b shows the updated building mask with the identified bridge areas removed. These buildings have been highlighted in the original image by the use of a red circle. It is an encouraging outcome of this research that no buildings were falsely identified as a bridge, in either data set, thus suggesting that the method will be effective in improving building detection rates.

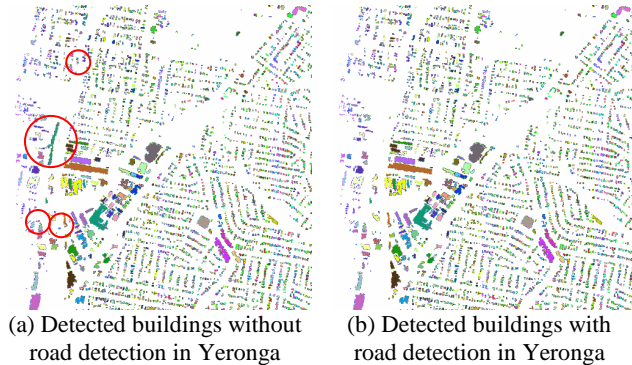


Figure 5. Building detection can be improved by first considering the road network.

#### 4.5 Road Vectorisation and Determination of Profiles

The vectorised centrelines of the detected roads from both data sets are found in Figure 6. The roads were vectorised as described in Section 3.1, ultimately providing a traced road centreline network that can be used to form longitudinal profiles and cross sections of the road network.

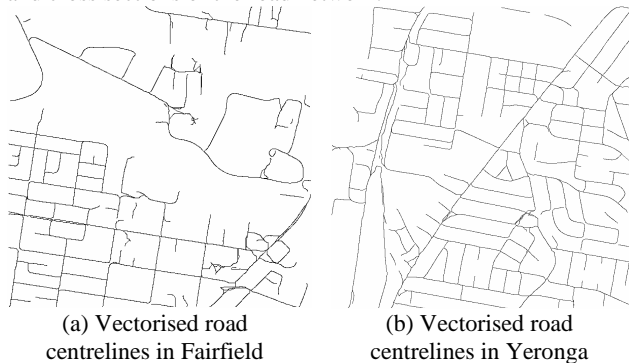


Figure 6. Vectorisation using the PCD and tracing algorithm.

The vectorised network provides a good representation of the detected road network as shown in Figure 7. The quality of the vectorised centreline results are summarised in Table 3 as described by Wiedemann (2003). One problem area that needs to be worked on is the modelling of the vectorisation process at a round-about as described in Figure 7b. The extracted centrelines have been used to generate the longitudinal profiles and cross sections of the road network as displayed in Figure 8. Elevations have been taken from the last-pulse *DSM*.

	RMS	Completeness	Correctness
Fairfield	1.48	0.86	0.69
Yeronga	1.42	0.79	0.83

Table 3. Quality results from the vectorisation process as described in Wiedemann (2003) with a buffer width of 2 metres.

#### 4.6 Discussion

In order to analyse the results carefully, the spatial distributions of the results are plotted in Figure 9 displaying the TP, FN, FP and True Negatives (TN) pixels in yellow, blue, red and white respectively. Both data sets show a very good correlation

between the detected and ground truth. The Yeronga data set is missing quite a few segments that are displayed in blue in Figure 9 and also reflected in the low completeness numbers in Table 1. The reason why these sections are missing is that there were several small regions in each missing section that had been stopped because of one of the criteria. Unfortunately, each of these small regions did not meet the requirements for the minimum size and hence were removed from the detected image displayed in Figure 2d.

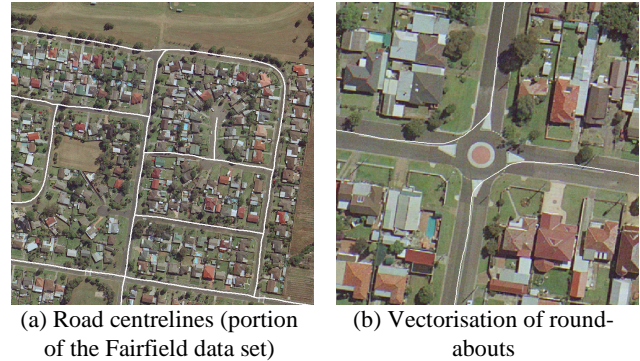
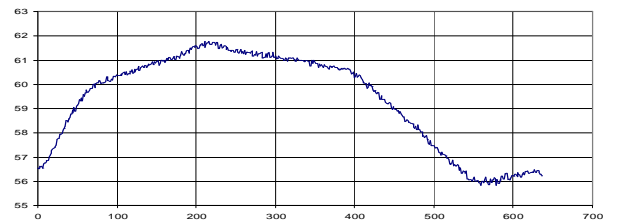
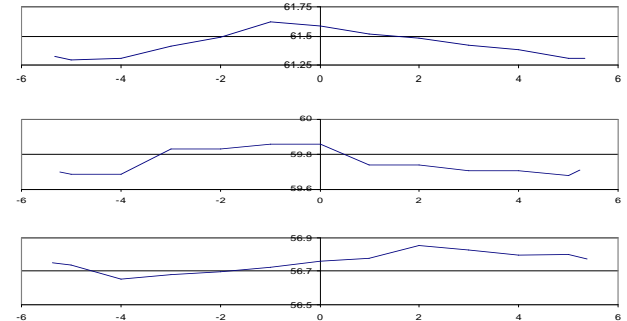


Figure 7. Vectorisation overlaid on the orthophoto.



(a) The automatically generated Longitudinal Section



(b) Cross sections along Figure 9a at 200m, 300m and 400m.

Figure 8. An example of automatically generated profiles



Figure 9. Spatial distribution of errors

The majority of the false positives can be attributed to carparks with one notable exception. In the Yeronga data set, there is a long road-like structure visible on the western side of the image running approximately North-South. This area is actually a railway line that has been detected by the algorithm as it has

many of the same properties as a road. The detection of the railroad here is the reason why bridge 11 has been detected as displayed in Figure 3b.

The automatic generation of longitudinal profiles and cross sections yielded surprisingly good results as displayed in Figure 8. The results appear a little noisy but the noise in general is in the order of  $\pm 5\text{cm}$  which is within the working limits of a LIDAR system. These results could be improved by applying a low pass filter over the values to smooth the end results. The quality of the detected road width appears very good except in areas near intersections. This problem is overcome by applying a low pass filter to the widths before the road edges are calculated.

## 5. CONCLUSION

This paper highlights the complexity of extracting features from LIDAR data. Many spatial objects to be recognised within a scene have very similar traits, making it extremely difficult to differentiate between object classes. This paper has shown that by combining different detection techniques the overall quality of existing algorithms can be improved, thus ultimately providing a better city model. Future work in city model creation should concentrate on developing ontologies for objects that need to be classified within an urban scene. Once the ontology is defined better algorithms can be developed.

Future algorithmic work will be concentrated on two distinct areas. Firstly the detection algorithm can be improved in 2 ways, namely by making the algorithm more robust so that no detected road segments are removed when removing small noisy areas, and by making the algorithm less dependant on thresholds. Although most of the parameters are data dependant others need to be calculated a-priori based on the road properties. It would be desirable to be able to approximate these thresholds based on the data itself. The second major area of improvement that has been identified is the vectorisation model used in the occurrence of a round-about. The current tracing algorithm will enter the round-about and exit immediately and then do a similar thing from the other side. Due to the blanking nature of the algorithm, the two road components, although representative of their road section appear incorrectly as disconnected road sections.

## ACKNOWLEDGEMENTS

This research was funded by ARC Linkage Project LP0230563 and ARC Discovery Project DP0344678. Both the Fairfield and Yeronga data sets were provided by AAMHatch, Queensland, Australia. (<http://www.aamhatch.com.au>)

## REFERENCES

- Akel, N. A., Zilberstein, O., Doytsher, Y., 2003. Automatic *DTM* extraction from dense raw LIDAR data in urban areas. In: Proc. FIG Working Week <http://www.ddl.org/figtree/pub/> (accessed 20 Feb. 2004).
- Auclair-Fortier, M.-F., Ziou, D., Armenakis, C., and Wang, S., 2001. Survey of work on road extraction in aerial and satellite images, *Canadian Journal of Remote Sensing*, 27(1): pp. 76-89.
- Brunn, C., Weidner, U., 1997. Extracting buildings from digital surface models. In: *IAPRS XXXII / 3-4W2*, pp. 27-34.
- Clode, S. P., Zelniker, E. E., Kootsookos, P. J., Clarkson, I. V. L., 2004a. A phase coded disk approach to thick curvilinear line detection, In: *Proceedings of EUSIPCO*, Vienna, Austria, pp 1147-1150.
- Clode, S., Kootsookos, P., Rottensteiner, F., 2004b. The Automatic Extraction of Roads from LIDAR Data. In *IAPRSIS XXXV-B3*, pages 231 – 236.
- Clode, S. and Rottensteiner, F., 2005. Classification of trees and powerlines from medium resolution airborne laserscanner data in urban environments. In *WDIC*, Vol. 1, pp. 191-196.
- Duda R., Hart P.E., 1972. Use of the Hough transform to detect lines and curves in pictures, *Comm Association of Computing Machines*. 15(1), pp. 11–15.
- Fuchs, C., Gülch, E., and Förstner, W., 1998. OEEPE survey on 3D - city models. OEEPE Official Publication 35, pp. 9-123.
- Haala, N. and Brenner, C., 1999. Extraction of buildings and trees in urban environments. *ISPRS Journal of Photogrammetry and Remote Sensing*, Vol. 54, pp. 130-137.
- Hatger, C., Brenner, C., 2003. Extraction of road geometry parameters from laser scanning and existing databases, *Int'l Archives of the Photogrammetry, Remote Sensing and Spatial Information Sciences*, Vol. XXIV, Part 3/W13,.
- Heipke, C., Mayer, H., Wiedemann, C., Jamet, O., 1997. Evaluation of automatic road extraction. In: *Int'l Archives of Photogrammetry and Remote Sensing*, Vol. XXXII, pp. 47–56.
- Hinz, S., Baumgartner, A., 2003. Automatic extraction of urban road networks from multi-view aerial imagery. *ISPRS Journal of Photogrammetry and Remote Sensing*, 58/1-2:83 –98.
- Kraus, K., 2002. Principles of airborne laser scanning, *Journal of the Swedish Society of Ph & RS*, 1, 53-56.
- Rieger, W., Kerschner, M., Reiter, T. and Rottensteiner, F., 1999. Roads and Buildings from Laser Scanner Data within a Forest Enterprise. In: *International Archives of Photogrammetry and Remote Sensing*, Vol. XXXII, La Jolla, California, pp. 185 – 191.
- Rottensteiner, F., Briese, C., 2002. A new method for building extraction in urban areas from high-resolution LIDAR data. In: *IAPRSIS*, Vol. XXXIV / 3A, pp. 295-301.
- Rottensteiner, F., Trinder, J., Clode, S., Kubik, K., 2003. Building detection using LIDAR data and multispectral images. In: *Proceedings of DICTA*, Sydney, Vol. 2, pp. 673-682.
- Vosselman, G., 2002. On the estimation of planimetric offsets in laser altimetry data. *Int'l Archives of the Photogrammetry, Remote Sensing and Spatial Information Sciences*, Vol. XXXIV/3A, pp. 375–380.
- Wiedemann, C., 2003. External Evaluation of Road Networks. In: *International Archives of Photogrammetry and Remote Sensing*, Vol. XXXIV, pp. 93–98.
- Zhang, C., 2003. *Updating of cartographic road databases by image analysis*. PhD dissertation. Mitteilungen Nr 79 of the Institute of Geodesy and Photogrammetry at ETH Zurich, Switzerland.